2,2′-Dihydroxybenzophenones and their carbonyl N-analogues as inhibitor scaffolds for MDR-involved human glutathione transferase isoenzyme A1-1

Fereniki D. Perperopoulou [a], Petros G. Tsoungas [b], Trias N. Thireou [c], Vagelis E. Rinotas [d], Eleni K. Douni [c,d], Elias E. Eliopoulos [c], Nikolaos E. Labrou [a], Yannis D. Clonis [a,*]

[a] Laboratory of Enzyme Technology, Department of Biotechnology, Agricultural University of Athens, 75 Iera Odos Street, GR-118 55 Athens, Greece
[b] Department of Biochemistry, Hellenic Pasteur Institute, Athens, Greece
[c] Laboratory of Genetics, Department of Biotechnology, Agricultural University of Athens, Athens, Greece
[d] Division of Immunology, Biomedical Sciences Research Center 'Alexander Fleming', Vari, Greece

ABSTRACT

The MDR-involved human GSTA1-1, an important isoenzyme overexpressed in several tumors leading to chemotherapeutic-resistant tumour cells, has been targeted by 2,2′-dihydroxybenzophenones and some of their carbonyl N-analogues, as its potential inhibitors. A structure-based library of the latter was built-up by a nucleophilic cleavage of suitably substituted xanthones to 2,2′-dihydroxy-benzophenones (5–9) and subsequent formation of their N-derivatives (oximes 11–13 and N-acyl hydrazones 14–16). Screening against hGSTA1-1 led to benzophenones 6 and 8, and hydrazones 14 and 16, having the highest inhibition potency (IC$_{50}$ values in the range 0.18 ± 0.02 to 1.77 ± 0.10 μM). Enzyme inhibition kinetics, molecular modeling and docking studies showed that they interact primarily at the CDNB-binding catalytic site of the enzyme. In addition, the results from cytotoxicity studies with human colon adenocarcinoma cells showed low LC$_{50}$ values for benzophenone 6 and its N-acyl hydrazone analogue 14 (31.4 ± 0.4 μM and 87 ± 1.9 μM, respectively), in addition to the strong enzyme inhibition profile (IC$_{50(6)}$ = $1,77 \pm 0.10$ μM; IC$_{50(14)}$ = 0.33 ± 0.05 μM). These structures may serve as leads for the design of new potent mono- and bi-functional inhibitors and pro-drugs against human GTSs.

© 2014 Elsevier Ltd. All rights reserved.

1. Introduction

Benzophenones, constitute a major class of compounds found in the Clusiaceae (or Guttiferae) family of plants, along with xanthones, coumarins and biflavonoids, having multiple biological activity.[1] o-Hydroxybenzophenone derivatives, in particular, are ubiquitous in naturally occurring and synthetic compounds.[1] The presence of the ortho-hydroxy diaryl ketone entity in many biologically active compounds and natural products makes it a privileged structure in medicinal chemistry and a synthesis target. Well-known and important members are the combretastatins and phenstatins.[2]

Functionalized 2-hydroxybenzophenones have been obtained from chromones, 3-formyl derivatives being most frequently used.[3] Inverse-electron-demand Diels–Alder reactions have been described, furnishing xanthones and 2-hydroxybenzophenones in low to moderate yields.[4] A catalyst-free cascade sequence has been reported for the synthesis of multi-functionalized 2-hydroxybenzophenones from electron deficient chromones. [5]

Unsymmetrically substituted and congested hydroxybenzophenone derivatives have been reported, PKA inhibitor balanol[6] or G6Pase inhibitor mumbaistatin[7] being two prominent examples. It is known that the reactivity and biological activity of hydroxybenzophenones is linked to their acid-base and metal chelating properties.[8] It is also known that their pharmacology is usually exerted through direct interaction with metal-bearing active enzyme sites.[9] It is reasonable to assume that the carbonyl and the o-hydroxyl groups are major determinants of this activity. Our recently reported interest in utilizing the reactivity profile of xanthone[10] in synthesis,[11,12] as well as its inhibitory potential towards GST,[13] prompted us to investigate its ring-opened analogue, substituted 2,2′-o-dihydroxybenzophenones, towards GST, taking advantage of their structure similarities, in pursuit of a potent inhibitor against hGSTA1-1 involved in multiple drug

resistance (MDR). To this end, GSTs (EC 2.5.1.18), a family of medically important isoenzymes that catalyse the conjugation of glutathione (GSH) to a variety of hydrophobic xenobiotic compounds, have been drafted. This enzyme family renders hydrophilicity to these xenobiotics, facilitating their metabolic processing and eventual secretion from the cell.[14] Cytosolic GSTs are found as homodimers or heterodimers.[15] Each monomer has an α/β domain and a large α-helical domain. The former domain contains the GSH binding site (G-site) on top of the large α domain. Between the two domains lies a hydrophobic pocket (H-site) in which the hydrophobic substrate (e.g., xenobiotic) binds and reacts with GSH. Since the produced conjugates are susceptible to further modification and eventual secretion from the cell, the GSTs are involved in major detoxification mechanisms of the cell from several xenobiotics and drugs. Based on exactly the same detoxification mechanisms, cancer cells may acquire resistance by overexpressing GST activities,[16] thus, hampering the effectiveness of certain chemotherapeutic drugs. Therefore, several drugs and prodrugs, acting as inhibitors against GSTs, have been proposed to overcome MDR attributed to GST overexpression.[17] GST-inhibiting strategies, focusing on ethacrynic acid analogues,[18] individual compounds[17,19] and prodrug molecules[20,21] have been employed. Several GSH analogues have also been proposed as more specific GST inhibitors,[22] exploiting the high affinity of GSTs for the tripeptide substrate GSH. An alternative concept exploits the susceptibility of GSH conjugates (products of GST catalysis) against the GSH-degrading enzyme γ-glutamyltranspeptidase (γGT) and eventually certain peptidase-stable GSH analogues have been put to the test as GST inhibitors.[23,24]

To the best of our knowledge, this is the first report on 2,2'-dihydroxybenzophenones and their carbonyl N-analogues as inhibitors against the MDR-involved human GSTs. Following GST inhibition screening, in silico molecular docking and enzyme inhibition kinetics, analogues exhibiting satisfactory inhibitory potency would be regarded as 'leads' in designing new inhibitors and respective prodrugs for human GSTs of medical importance.

2. Results and discussion

2.1. Chemistry

2.1.1. Synthesis

Benzophenones, carrying hydroxyl groups *ortho*-disposed to the carbonyl group, interfere in various transformations, thus, necessitating their protection and subsequent deprotection. Clearly, this is a serious drawback in any synthetic scheme diminishing their potential. The nucleophilic cleavage of xanthone of type **4** (Scheme 1) serves as a useful alternative route. The two benzene rings of **1** are identical, imparting symmetry elements to the structure. It is, thus, the substitution pattern on **1** that dictates the corresponding one of **5**. Unsubstituted or symmetrically and asymmetrically substituted derivatives of **5**, exist as a single regio-isomer. Apparently, this is so, because the incorporated cleaving alkali can occupy either one of the alternative ring opening sites, ending up *ortho*-disposed to the carbonyl group.

The generation of the core structure **5** from the pyran C—O bond cleavage of **4** has long been known.[25] Indeed, the cleavage to **5** may be accomplished, under mild conditions, using coordination complexes of **1** with transition metals (Cr, Fe, Ir)[25] or using strong alkali, under either mild[25] or forcing conditions.[11,12] The cleavage, under mild conditions, suffers from complications, such as generation of the coordination complex of **1** and ultimate removal of the metal part in the former method or removal of the activating NO₂ group in the latter one. On the other hand, cleavage, under forcing conditions, despite its obvious drawback, does lead directly to the
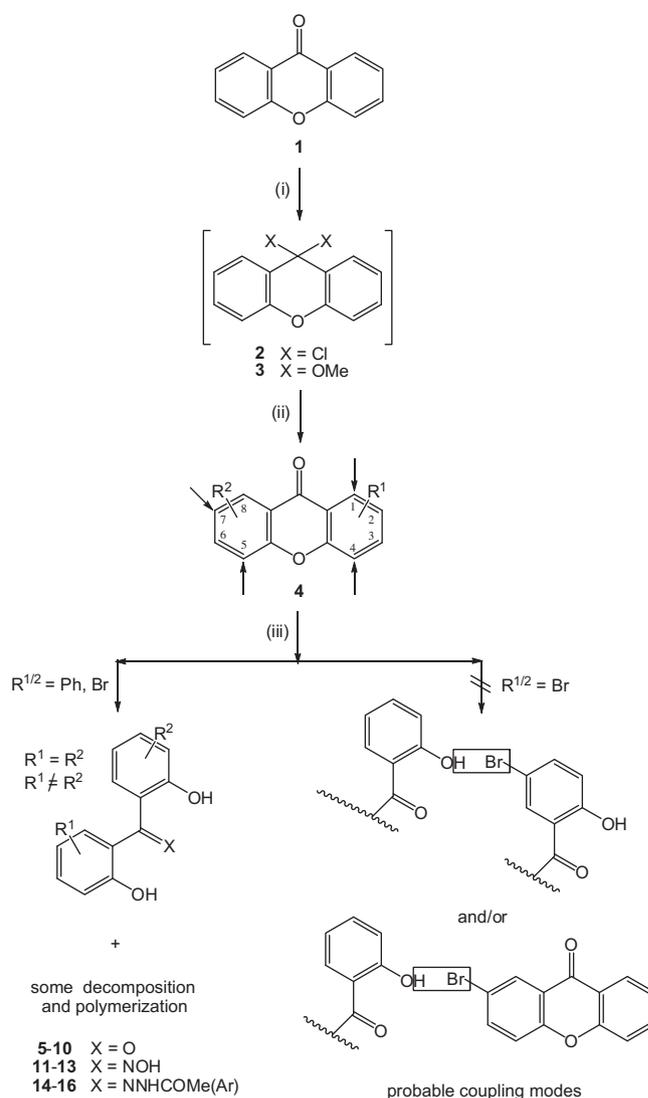
Scheme 1.

desired **5**. Indeed, a recently reported protocol[10] addressed this issue, taking advantage of the reactivity profile of **1**. Consequently, the direct cleavage of **4**, is a synthetically useful route in that it allows access to regioselectively and diversely substituted diaryl ketones **5**. The forcing conditions can be offset by the potential of any further desired functionalization on the regioselectively substituted **5–9**, either on the aryl rings or on the carbonyl moiety. Eventually, this has been adopted as the method of choice and derivatives **5–16** have been prepared for the objectives of the present work (Table 1).

The cleavage of (di)bromo-substituted **4** merits a special commentary (Scheme 1). The cleaving KOH has been used as a nucleophile in the conversion of aryl halides to phenols through various metal-catalyzed protocols.[26] Furthermore, KOH/DMSO, acting as a superbase, has been recently found[27] to effect the cross-coupling of a phenol with an aromatic halide, under mild conditions. In our case, however, using this reagent for the ring opening of **4**, no coupling product of any kind has been isolated. Instead, the reaction gave the expected benzophenone of type **2** in 73% yield, along with some intractable material. It is assumed that an intramolecular H bonding, engaging one of the phenol OH groups of **8** or **9** and the distorted conformation of these structures hamper any homo-(with **8** or **9**) or hetero-coupling (with their precursor **4**) through their bromine-bearing sites.

Table 1

The 2,2′-dihydroxybenzophenones and their *N*-carbonyl analogues of the present study and their hGSTA1-1 inhibition potency; ketones **5**–**10**; ketoximes **11**–**13**; *N*-acyl hydrazones **14**–**16**

Compound number[a]	Structure	Molecular formula	Molecular weight	Inhibition potency against hGSTA1-1[b] (%)
5		$C_{13}H_{10}O_3$	214	0
15		$C_{19}H_{16}N_3O_3$	334	31.8
7		$C_{25}H_{18}O_3$	366	33.9
11		$C_{13}H_{11}NO_3$	229	40.5
12		$C_{13}H_{10}BrNO_3$	308	52.3
9		$C_{13}H_8Br_2O_3$	372	58.6
13		$C_{19}H_{15}NO_3$	305	67.7
10		$C_{27}H_{21}BrO_3$	473	68.8
6		$C_{19}H_{14}O_3$	290	86.1

Table 1 (continued)

Compound number[a]	Structure	Molecular formula	Molecular weight	Inhibition potency against hGSTA1-1[b] (%)
14		$C_{20}H_{16}N_2O_3$	332	87.4
8		$C_{13}H_9BrO_3$	293	87.7
16		$C_{15}H_{13}BrN_2O_3$	349	96.1

[a] In ascending order of inhibition potency against hGSTA1-1.
[b] Mean value of three enzyme assays (25 μM analogue; error ⩽ 3%).

Worth noting is the direct derivatization of **5**–**9** to the oximes **11**–**13** and the hydrazones **14**–**16**, without the need of a protection–deprotection protocol. Intramolecular H bonding, partly masking the OH groups while increasing the electrophilicity of the carbonyl site, may serve as a satisfactory rationale for this outcome.

2.1.2. Structure

The structure of the parent **5** has been investigated by X-ray crystallography,[28] NMR (^1H, ^{13}C and ^{17}O) and FT-IR spectroscopy[29,30] as well as DFT-B3LYP/6-31G* calculations.[30] Compound **5** exhibits a lower than C_2 symmetry having its two phenol rings twisted out of the carbonyl plane by ca. 38°.[28] The deviation from planarity is sterically triggered by the relative orientation of the aryl rings.

X-ray and neutron-based multipolar and topological analyses have measured electron distribution in the Resonance-Assisted H-Bonded (RAHB) pseudo-ring conformation of 2-hydroxybenzophenone analogues.[31] Formal charges detected on the donor and acceptor O and N atoms as well as on the H bond-engaged H atoms have been rationalized by electrostatic and covalent interactions.

Substitution on the rings of **5** (one or both) will, expectedly, cause a further distortion of the structure. Indeed, this has been observed by geometry optimized calculations (MAGE v.6.44 programme) on the ketones **5**–**9**, oximes **11**–**13** and hydrazones **14**–**16** (parent **5** is included as the reference structure). The novel structures **6**–**16** (Table 1) have a molecular framework composed of a C = X moiety [**5**–**10**, X = O; **11**–**13**, X = NOH; **14**–**16**, X = HNNC-OAr (Ar: Ph, Py, Me)] bridging two phenols with their OH groups *ortho*-disposed to the bridge. The carbonyl and the phenol hydroxyl groups, are set to develop intramolecular or intermolecular H-bonding or other non-covalent bonding (e.g., π–π stacking, hydrophobic or halogen) interactions with the surroundings. A substantial torsion has been found in **5** (angles of ca. 35–55°) to minimize repulsion among the aromatic rings leading to a non planar conformation.[32] In our case, this is reflected on the intramolecular H bonding with only one of the OH groups.

All structures take up a twisted conformation (a twist angle of ca. 50° of the aryl rings around the carbonyl centre), in which the two rings are not coplanar while the carbonyl or its N-derivatives lie outside an obtuse valency angle in the range of 125–135°, indicative of a strained conformation. Both OH groups are, thus, not aligned for a notable intramolecular OH···O H-bonding interaction with the carbonyl centre. In fact, that of the unsubstituted ring forms a weak intramolecular H bond (Table 2) whereas the other one cannot be engaged in any at all.

Indeed, a H bonding, in the range of 1.992–1.934 Å, is found in **5**, **8** and **9** and none in **6** and **7**. The former is found to be ca. 0.2 Å longer (weaker) than earlier calculations on **5**[28] or its singly substituted 2-hydroxy-analogue.[31] A C=O length of ca. 1.216 Å, remains unaffected by H bonding and is virtually that of benzophenone.[33] Furthermore, there seems to be no change on this bond length upon blocking the OH groups. The bonds linking the carbonyl with the aryl rings appear to have the same length of ca. 1.475 Å. This bond length also reflects a virtually similar extent of conjugation of each of the rings with the carbonyl. Larger torsion angles in **5**–**9** are those of the substituted ring to relieve strain.

Analogous H bonding-related geometry features are demonstrated by oximes **11**–**13** and hydrazones **14**–**16**. NOH···O and OH···NN H bonding of magnitude similar to that of ketones is found in **12**, **15** and **16** while a much weaker in **14** and none in **11** and **13**. A C=N length of 1.304 Å for **11**–**13** and 1.307 Å for **14**–**16**, marginally affected by H bonding or substitution, indicates an elongation of ca. 0.15–0.25Å. A N–O elongation of ca. 0.15 Å in **11**–**13** or an N–N one of 0.30 Å in **14**–**16**, is also observed. A N–HN···H bonding of 2.487 Å in **15**, engaging the pyridine N, 'locks' the pyridine orientation, thus, the conformation of the whole structure. In addition, the O–H length in both phenol rings remains unchanged throughout the series. The bonds linking the imine centre with the aryl rings appear to be of ca. 1.479–1.480 Å, slightly longer than their precursors **5**–**8**. Torsion angles appear to be affected by substitution but rather more significantly by the N–O repulsion of the oxime or hydrazone N lone pair and phenol OH groups.

Table 2
Bond lengths (Å) and dihedral angles ω (degrees) of **5–16**

Compound number	O—H	(C)O···H	$d_{O\text{-}O}$[a]	ω	N—O-H	O-H···N	N—O···H—O	C=O	C=N	NH···N
5[b,c]	0.988[d]	1.711[d]	2.587[d]	34.2/52.6[f]				1.216		
	0.966/7	1.992	2.742							
	0.984[e]	1.768[e]								
6	0.966/7	>3	>3	41.6/42.7				1.217		
7	0.966/7	>3	>3	38.2/33.8				1.215		
8	0.966/7	1.934	2.701	36.1/53.2				1.216		
9	0.966/7	1.976	2.718	32.7/53.2				1.216		
10		>3	2.642					1.216		
			$d_{N\text{-}O}$							
11	0.966/7	>3		43.3/43.5	0.969	2.960	1.944		1.304	
12	0.966/7	2.689		55.5/51.3	0.968	1.933			1.304	
13	0.966/7	>3		41.1/44.4	0.968	>3			1.304	
14	0.966/7	>3		43.6/52.8		2.067			1.307	
15	0.966/7	2.698		47.6/55.0		1.936			1.307	2.487
16	0.966/7	2.716		37.6/54.7		1.944			1.307	

[a] Shortest distance is recorded.
[b] B3LYP/6-31G* calculations.
[c] HF/6-31G* calculations.[30]
[d] Dávalos, J. Z.; Guerrero, A; Herrero, R.; Jimenez, P.; Chana, A.; Abboud, J.L.M.; Lima, C. F.R.A.C.; Santos, L.M.N.B.F.; Lago, A.F. *J. Org. Chem.* **2010**, *75*, 2564.
[e] 2-Hydroxybenzophenone [Krygowski, T.M.; Zachara-Horeglad, J.E.; Paluciak, M. *J. Org. Chem.* **2010**, *75*, 4944].
[f] ω values refer to unsubstituted (left) or substituted (right) aryl rings, respectively.

Consistent with the nature and strength of the H bonding are their ir, ^{1}H and ^{13}C NMR spectra. Ir absorptions in the range of 1620–1615 cm^{-1} for the C=O group and 3450–3200 cm^{-1} for the OH groups, were observed. Further, lowfield distinct ^{1}H signals at δ = 10.64, 10.50 and 10.48 ppm for the OH groups and ^{13}C signals at δ = 201–199 ppm for the C=O group appeared. The facile direct derivatization of ketones **5–9** to **11–16** is of interest, as it lends further support to the H bonding mode (see earlier section). The experimentally and computationally derived values are in good agreement with earlier results on **5**[28,30] or its singly substituted 2-hydroxy-analogue.[31] They also fall within the ranges commonly reported in functional group databases.

Based on the presented data, the following features emerge: (a) bromo substitution (whether mono-**8** or di-**9**) has a negligible effect on the conformation (**5**, **8** and **9** assume virtually the same conformation), (b) a marked distortion by a substantial twist is observed in the corresponding phenyl-substituted derivatives **6** and **7**, particularly so in the latter, (c) the phenyl mono-substituted derivatives **6** and **13** also assume a similar conformation, (d) substitution pattern and H bonding have an effect on the flexibility and shape of the structures, (e) lone pair N–O repulsion in **11–13** or in **14–16**, only to a lesser extent, is probably a determinant for the observed conformations though a weak one ($d_{N\text{-}O}$ 2.7–3.4 Å).

2.2. Screening of the compounds and selection of 'lead structures' as hGSTA1-1 inhibitors

Before embarking into the inhibition studies we performed control experiments with our enzyme preparation using bromosulf-ophthalein (BSP) as a known hGSTA1-1 inhibitor.[34] In silico molecular modeling and docking analysis predicted that BSP binds to a non-catalytic site, allowing simultaneous binding of the substrate CDNB to the catalytic primary site (**SM-1**). This is in agreement with earlier observations[34] and has been confirmed by kinetic studies with our enzyme preparation, using BSP as an inhibitor and CDNB as a variable substrate, demonstrating a non-competitive modality of inhibition.[13,19]

In designing the enzyme assay protocol for screening the compounds as potential hGSTA1-1 inhibitors, the concentration of 25 μM, falling within the 1–30 μM range, suggested in bibliography as an appropriate one for inhibitor screening,[35] has been chosen. A more crucial factor to be decided has been the substrate concentration, [CDNB], in the enzyme inhibition assay for the screening and IC$_{50}$ calculations. Having initially determined the Michael is constant, K_m, for the CDNB-hGSTA1-1 couple as 0.32 ± 0.08 mM, an experimental [CDNB] $\ll K_m$ would have given low values for [CDNB]/K_m. This assay condition would increase the apparent inhibition caused by a fixed concentration (25 μM in our hands) of a competitive inhibitor; hence, a low [CDNB], relative to K_m, favours the identification of competitive inhibitors.[35] In contrast, if we were to run the enzyme assays at relatively high substrate concentrations (i.e., high [CDNB]/K_m values), we would bias the screening assay against competitive inhibitors, in favour of uncompetitive ones, whereas the inhibition potency of non-competitive inhibitors would not be affected by the ratio outcome.[35] We have chosen to perform the enzyme inhibition assays under the so-called 'balanced assay conditions' (BAC) as the optimum choice, ensuring an experimental [CDNB] = 0.3 mM ≈ K_m.

In order to reveal their enzyme inhibitory potency all compounds were subjected to experimental screening against hGSTA1-1 activity. From the data obtained (Table 1), one distinguishes three groups of inhibitory potency: (a) low inhibition (up to ca. 34%; compounds **5**, **15** and **7**), (b) medium inhibition (ca. 34–69%; compounds **11**, **12**, **9**, **13** and **10**) and (c) high inhibition (above 86%; compounds **6**, **14**, **8** and **16**). BSP was also put to the test as a control inhibitor, under the same conditions and it was found to inhibit hGSTA1-1 by approximately 63%.[19] The encouraging behaviour of the 'high inhibition' compounds (Table 1; **6**, **14**, **8** and **16**) was confirmed experimentally by the low IC$_{50}$ values obtained from concentration–response curves (Table 3; as an example, see Fig. 1) and predicted by in silico studies. Molecular modeling and docking analysis of **6**, **14**, **8** and **16** with hGSTA1-1, in particular, provided an insight into salient structural features unveiled upon interaction. By inspecting the location of the most favourable conformations (i.e., low energy ones) of these compounds, docked in the hGSTA1-1 binding site, the following observations are evident. A clustering occurs on two locations in the binding area (Fig. 2), one in the proximity of the a-helix 155–169 (internal secondary pocket) and one in the proximity of the a-helix 210–220, where CDNB also binds (external catalytic pocket).

Upon generation of the enzyme complex, the geometry of the structures adjusts to achieving the best fit. It is, thus, expected that the weakly RAHB-stabilized conformers ('closed' or 'pseudo ring' form), that is, **5**, **8**, **9**, **12** and **14–16**, hiding polarity from the surroundings, render the structures weakly lipophilic. It follows that their acidic (OH and NH) groups take precedence over

Table 3
Behaviour of compounds selected from screening experiments (Table 1) against hGSTA1-1 activity (IC$_{50}$) and Caco2 cells (LC$_{50}$)

Compound number and structure	Modality of inhibition[a]	IC$_{50}$ against hGSTA1-1 (μM)	LC$_{50}$ against Caco2 cells (μM)
5	–	–	>400
6	Competitive, linear	1.77 ± 0.10	31.4 ± 0.4
8	Mixed, linear	0.24 ± 0.04	120 ± 1.9
11	–	–	315 ± 1.4
14	Competitive, linear	0.33 ± 0.05	87 ± 1.9
16	Mixed, hyperbolic	0.18 ± 0.02	>400
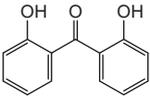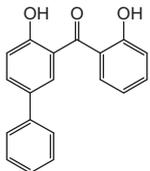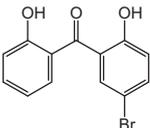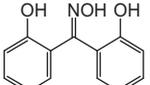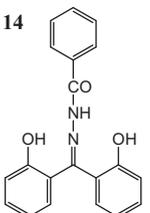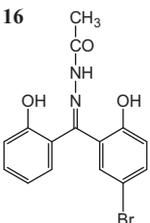
[a] Compounds **6**, **8**, **14** and **16** showed mixed inhibition modality with the co-substrate GSH.

intermolecular interactions in the enzyme environment through an accentuated hydrophilicity. Ring-substituent-triggered interactions should eventually rest upon and facilitate charge transfer pathways.[36] To that end, singly substituted ketones **6** and **8** or hydrazones **14** and **16** are highly efficient binders. Of these, the former, being unsymmetrically substituted, have an unequal charge distribution and greater flexibility, in contrast to their symmetrically disubstituted and sterically congested relatively poor binders **7** and **9**. Compounds **14** and **16** incorporate an acidic NH site and a hydrophobic *N*-acyl terminal group (Ph or Me). These features allow interactions, through a charge relay, within the protein cavity, determined by the polar side of helix 155–169, dispersed with charged (Glu162, Glu169) and polar (Tyr166) residues. The lower inhibitory performance of **15** may be attributed to its 'locked' conformation (see earlier), reducing its flexibility and eventually binding efficiency. Of the oximes, regardless of their E and/or Z conformation, **13** shows the highest inhibitory potency, followed by **12** and **11**, a trend similar to that of **5**, **8** and **9**. **10**, the

benzylated derivative of **5**, has been found to have a variable inhibitory potency. Masking both hydroxyl groups removes the intra-molecular H bonding. Any potential hydrophilic interactions, thus, facilitate mainly π–π (arene–arene) or intermolecular H bonding interactions, engaging the C=O group with the enzyme surroundings. The variability of its inhibitory potency has been tentatively attributed to its facile debenzylation in the enzyme cavity. From the clustering of the inhibitors on docking (Fig. 2), steric congestion (e.g., **7**), apparently enhanced by symmetrical substitution, as a parameter impeding proper fit, may serve as a selection rule for lead candidates.

2.3. Studying the modality of interaction between the selected inhibitor lead structures and hGSTA1-1

On the basis of the 'cherry picking' (screening) experiments and the low IC$_{50}$ values observed, enzyme inhibition kinetics on compounds **6**, **8**, **14** and **16** were performed in order to clarify their
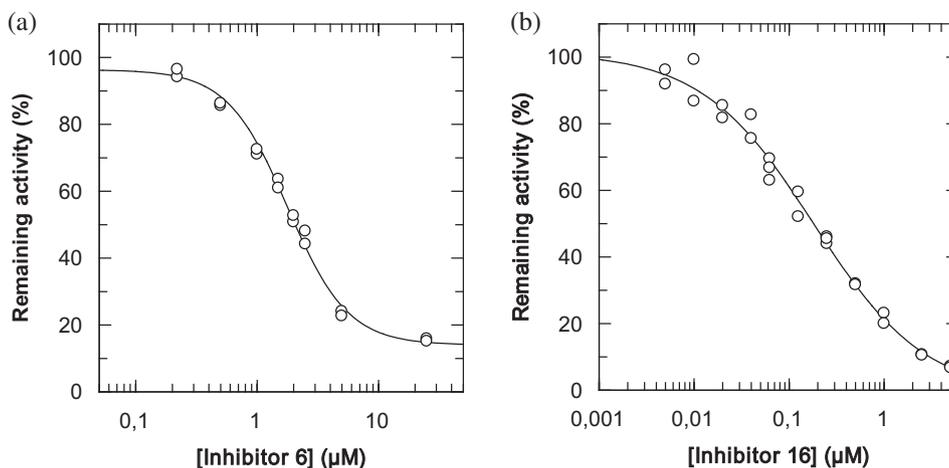
Figure 1. Concentration–response graphs for the determination of the IC_{50} values for **6** (a) and **16** (b) against hGSTA1-1. The 'concentration' values (µM) are presented on logarithmic scale, whereas the 'response' values (as% ratios of inhibited over uninhibited rates) are presented on the 'Remaining activity' axis. The graphs were produced using the GraFit3 v.3 computer program.
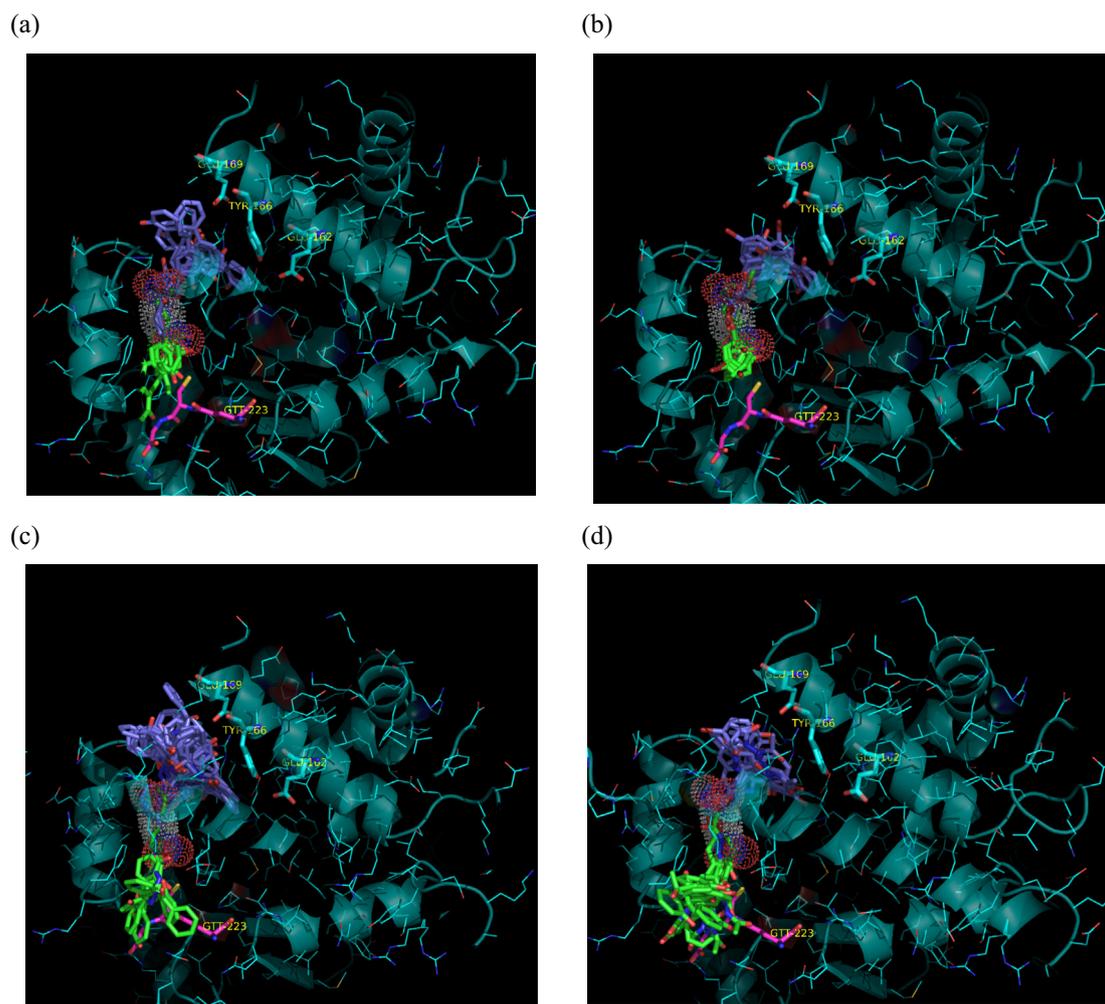
Figure 2. Clustering of the four selected inhibitors, **6** (a), **8** (b), **14** (c) and **16** (d) at the most probable binding positions on hGSTA1-1 as predicted by in silico molecular docking. It is evident that clustering occurs on two locations in the binding site, one in the proximity of the a-helix 155–169 (internal secondary pocket; upper) shown in purple and one in the proximity of the a-helix 210–220 where CDNB also binds (external catalytic pocket; down) shown in green. All ligands are depicted in sticks representation. The position where the substrate CDNB would bind in the absence of inhibitor is shown as space filling dot model. The co-substrate GSH is depicted in magenta, the S atom in yellow, N atoms in blue and O atoms in red. The figure is created using the PYMOL v1.5 program.
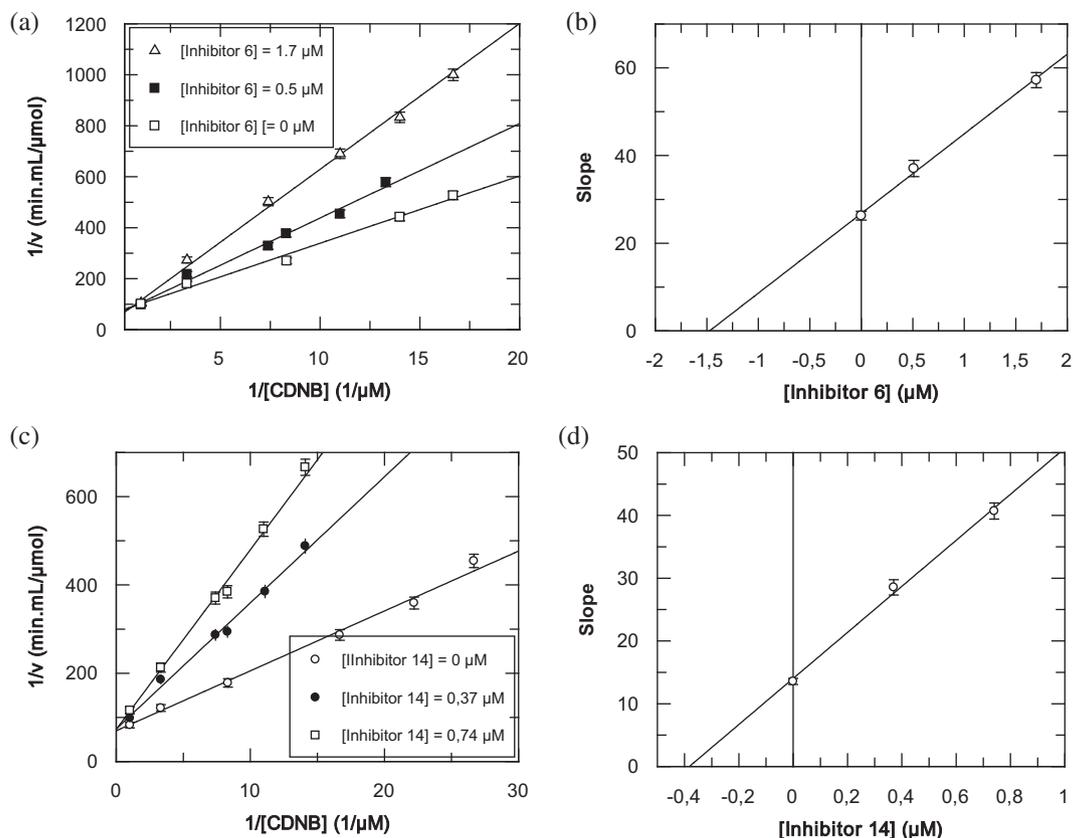
Figure 3. Purely competitive inhibition kinetics of hGSTA1-1 with inhibitors **6** (a and b) and **14** (c,d) using CDNB as a variable substrate. Lineweaver–Burk graphs of initial velocities of hGSTA1-1 versus [CDNB] (37.5–980 µM) at different concentrations of inhibitor **6** (a) and inhibitor **14** (c). Secondary graphs for **6** (b) and **14** (d) derived from data of respective primary graphs (a) for **6** and (c) for **14**. The inhibition constants $K_{i(6)}$ for **6** and $K_{i(14)}$ for **14** are the intercepts on the basis axes of graphs (b) and (d), respectively. Points are average of three enzyme assays. The graphs are created using the GraFit v.3 program.
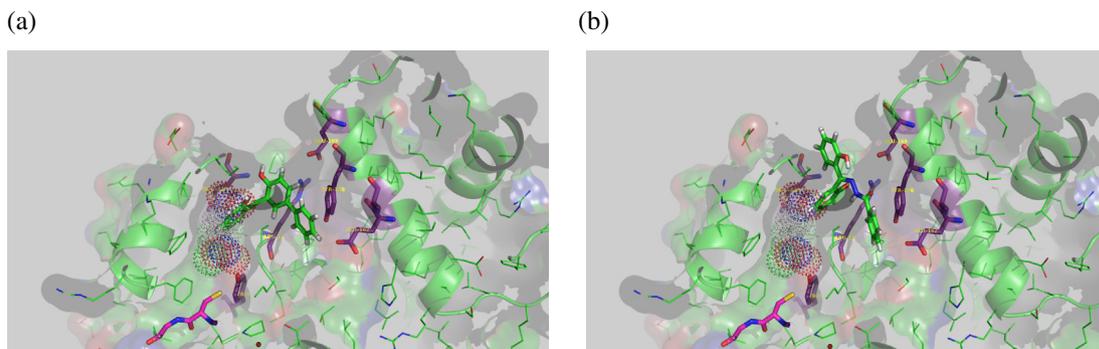
Figure 4. Low energy conformations of substrates CDNB, GSH and inhibitors **6** (a) and **14** (b) at the most probable binding sites of hGSTA1-1 as predicted by in silico molecular docking. All ligands are shown as balls-and-sticks, except for CDNB which is shown as space filling dot model. Both inhibitors (green ligands) partly occupy the catalytic site and clash with CDNB when bound at the same site. GSH is depicted in magenta, the S atom in yellow, N atoms in blue and O atoms in red. The figure is created using the PyMOL v1.4 program.

binding modality towards the target hGSTA1-1, a fundamental knowledge useful in inhibitor design. In all four cases, two sets of experiments were implemented, each employing either CDNB (37.5–0 980 µM) or GSH (100–2500 µM) as a variable substrate, in the presence of different steady inhibitor concentrations.

2.3.1. Study of inhibitors 6 and 14

When using CDNB as a variable substrate, **6** and **14** displayed purely competitive inhibition kinetics on the basis of the linearity observed for both the double reciprocal Lineweaver–Burk graphs (Fig. 3a for **6** and Figure 3c for **14**), at various steady concentrations of **6** and **14** and their respective secondary derivatives (Fig. 3b for **6**

and Figure 3d for **14**).[37,38] This behaviour suggests that these two inhibitors compete with CDNB for the same binding site of the enzyme; calculated inhibition constants $K_{i(6)} = 1.47 \pm 0.15$ µM (from Fig. 3b) and $K_{i(14)} = 0.38 \pm 0.05$ µM (from Fig. 3d). The described kinetic model is in concert with the in silico molecular docking analysis. The latter predicts that both inhibitors, **6** (Fig. 4a) and **14** (Fig. 4b), despite featuring different core structures, in their low energy most favoured position, they clash with CDNB, if trying to accommodate them at the catalytic site of hGSTA1-1 where CDNB binds. In this case, it appears that the binding modality (competitive or mixed) is not determined primarily by the inhibitor core structure (i.e., benzophenone, as in **6** and **8**

or its *N*-carbonyl hydrazone, as in **14** and **16**), but rather by the presence of bulky substituents (i.e., an aromatic group present on **6** and **14**, absent in **8** and **16**). This extra added volume forces **6** and **14** to adopt new orientations upon binding to hGTA1-1 (Fig. 4), eventually leaving not enough space for a simultaneous binding of CDNB at the same binding site.

With GSH as a variable substrate, both **6** and **14** showed mixed inhibition kinetics, manifested by the lines of the double reciprocal Lineweaver–Burk graphs of hGSTA1-1 versus [GSH] initial velocities, at various steady concentrations of **6** and **14**, not intersecting the reciprocal velocity or [GSH] axes (**SM-2a**).[37,38] Furthermore, the linear correlation of the respective secondary graphs, depicting slope versus [inhibitor] (**SM-2b**), is supportive of a purely mixed type of inhibition.[37,38] The equilibrium model for this type bears the assumption that the inhibitor binds to both the free *enzyme* and its *enzyme–GSH* complex, with no possibility for product formation[37,38] (the respective complexes are unreactive, 'dead-end'). The model suggests that inhibitors **6** and **14** may interact at a site other than the GSH-binding site of hGSTA1-1, that being partly the catalytic CDNB-binding site, as described earlier (Fig. 3).

2.3.2. Study of inhibitors 8 and 16

With CDNB as a variable substrate, **8** has shown mixed inhibition kinetics (cf **6**),[37,38] as manifested by the lines of the double reciprocal Lineweaver–Burk graph not intersecting the reciprocal velocity or [CDNB] axes (**SM-3a**) and the fair linearity observed for the respective secondary graph (**SM-3b**); $K_{i(8)} = 0.36 \pm 0.11$ μM. This inhibition modality rests upon an equilibrium model, which foresees no product formation, since the predicted *enzyme–8* and

enzyme–CDNB–8 complexes are the unreactive ('dead-end') ones.[37,38] However, at [**8**] >0.5 μM (e.g., 0.8 μM), the secondary plot curves upwards (**SM-4**), suggesting the binding of a second molecule of **8**, thus, intensifying its inhibitory effect.[38] This view is supported by earlier works[13,39,19,34] on the existence of multiple binding sites with GSTs for a single compound, often with varying affinity and inhibitory potency. Kinetic studies and isothermal titration calorimetry with the non-competitive inhibitor BSP and hGSTA1-1 pointed to two binding site types for BSP per enzyme subunit.[34,40] Furthermore, since BSP and CDNB bind the enzyme at different sites (**SM-1**), it has been proposed that the inhibition by BSP could be attributed to conformational/structural changes of the enzyme,[40] a modality of inhibition similar to that observed with **8**.

The parabolic mixed inhibition modality with a high [**8**], described above, assumes no catalytic activity for the *enzyme–inhibitor* and *enzyme–substrate–inhibitor* complexes,[37,38] and this is confirmed by molecular modeling and docking. The in silico models predict close proximity and interaction between the substrate CDNB and **8** (two H-bonds, 2.56 and 2.76 Å) when both bind the catalytic area of the enzyme (Fig. 5a and b). In this case, it is reasonable to anticipate interference of **8** with the enzyme's catalytic function involving CDNB. However, at higher [**8**], a second molecule of **8** is predicted to bind at the distant internal secondary site (**SM-5a**), intensifying the inhibition effect.

Turning to inhibitor **16**, with the CDNB as a variable substrate, one observes mixed inhibition kinetics, again, as shown by the lines of the Lineweaver–Burk graph intersecting left of the reciprocal velocity axis (Fig. 6a). However, the points of the
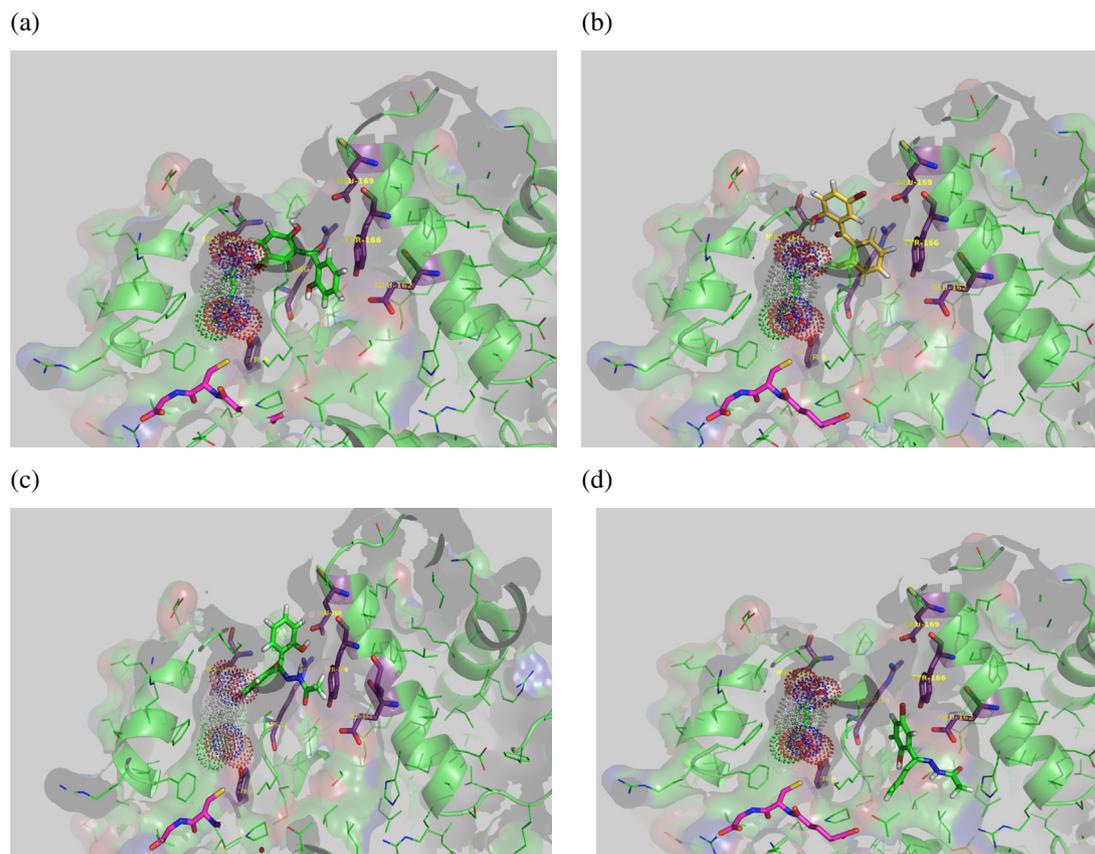
Figure 5. Low energy conformations of substrates CDNB, GSH and inhibitor **8** (a), (b) and inhibitor **16** (c), (d) at the most probable binding sites of hGSTA1-1 as predicted by in silico molecular docking in the absence and presence of CDNB. All ligands are shown as balls-and-sticks, except for CDNB which is shown as space filling dot model. (a) In the absence of CDNB, inhibitor **8** (green ligand) is bound close to CDNB-binding region. (b) In the presence of CDNB, inhibitor **8** (yellow ligand) is bound close to CDNB, developing H-bonds (2.56 and 2.76 Å). (c) In the absence of CDNB, inhibitor **16** (green ligand) is bound close to CDNB-binding region. (d) In the presence of CDNB, inhibitor **16** (green ligand) is bound far enough from CDNB (space filling dot model) permitting catalytic function, though at a lower rate. The co-substrate GSH is depicted in magenta, the S atom in yellow, N atoms in blue and O atoms in red. The figure is created using the PyMOL v1.4 program.
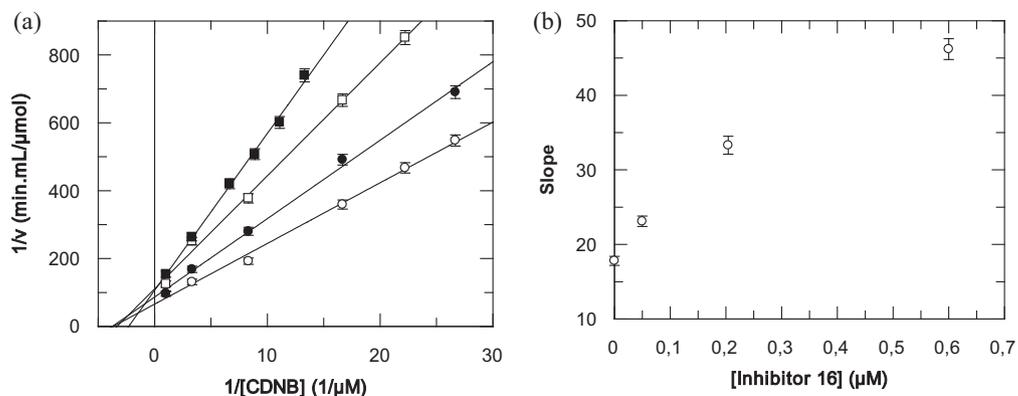
Figure 6. Mixed inhibition kinetics of hGSTA1-1 with inhibitor **16** using CDNB as a variable substrate. (a) Lineweaver–Burk graph of initial velocities of hGSTA1-1 versus [CDNB] (37.5–980 μM) at different concentrations of inhibitor **16** (○ 0, ● 0.05, □ 0.20 and ■ 0.60 μM). (b) Secondary graph derived from data of graph (a). Points are average of three enzyme assays. The graphs are created using the GraFit v.3 program.
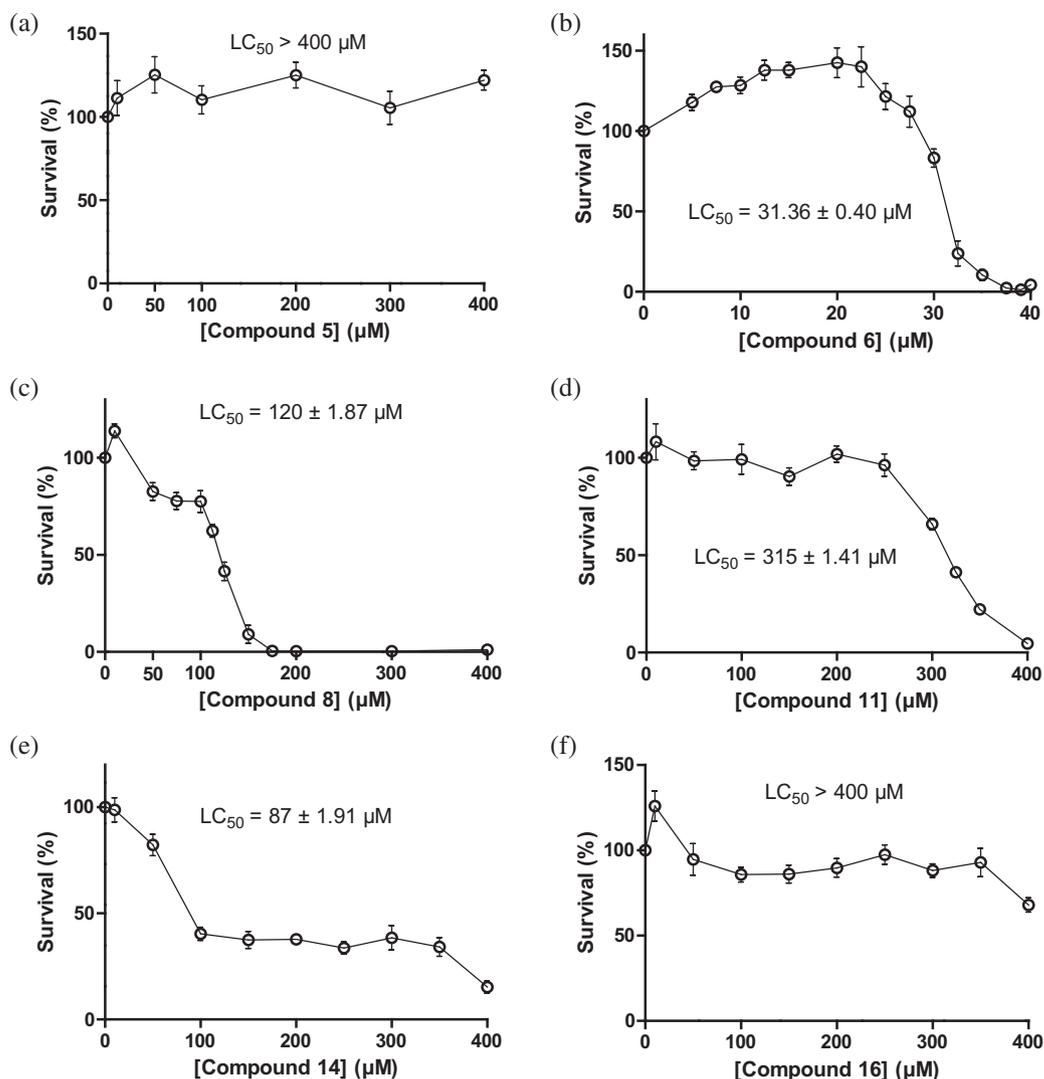
Figure 7. The effect of **5** (a), **6** (b), **8** (c), **11** (d), **14** (e) and **16** (f) on the viability of human colon adenocarcinoma (Caco2) cells after 24 h treatment. Cytotoxicity was assessed using a microplate MTT colorimetric assay. Survival (cell viability) was expressed as a percentage of the negative control without treatment with compounds. LC_{50} values are given as mean + SEM from three independent experiments performed in triplicate. The graphs were produced using the GraphPad PRISM v.5 computer program.

secondary graph, derived from data of Figure 6a, curve downwards to a limiting rate (Fig. 6b), suggesting a hyperbolic mixed inhibition modality.[38] These findings predict[37,38] that **16** binds to both the *free enzyme* and the *enzyme–CDNB* complex, leading to formation of at least two complexes, *enzyme–16* and *enzyme–CDNB–16*, respectively. A GSH molecule should be present onto both complexes (not shown) due to using an enzyme-saturating GSH concentration in the respective assays. In contrast to the modality described for **8**, the present model predicts a breakdown of the *enzyme–GSH–CDNB–16* complex to products, at a rate slower than that without inhibitor.[37,38] On the basis of these experimental findings, it is reasonable to assume that, in the presence of CDNB, **16** binds to a site where there can be no direct and detrimental to the catalytic function interaction between them, thus, allowing a reduced catalytic function. This is in concert with in silico molecular docking, showing CDNB at the catalytic primary site (Fig. 5d, left) and **16** at a distant secondary site (Fig. 5d, right) of hGSTA1-1, as the two most probable binding ones, respectively, producing a reactive quadruple complex, *enzyme–GSH–CDNB–16*. Apparently, these locations are not close enough (**SM-5b**) for **16** to abolish the enzyme's catalytic function on CDNB, as observed with **8**.

In summary, to accommodate **8** or **16** in hGSTA1-1, simultaneously with CDNB while **8** should first be fixed at the most probable position in the catalytic (primary) site, followed by a second molecule, taking up a position in the distant (internal) secondary site,[19] located on the a-helix 86–109 side (**SM-5a**), the larger **16** binds only as a single molecule at the distant (internal) secondary site (**SM-5b**). This is, indeed, demonstrated by a very narrow clustering of probable positions for the inhibitors, indicating the volume limitations and shape restrains for the available protein cavity.

Because of the non-linearity observed with the secondary graph (Fig. 6b), the $K_{i(16)}$ was calculated from linear double reciprocal graphs, depicting 1/ΔSlope versus 1/[**16**] (**SM-6a**) and 1/ΔIntercept versus 1/[**16**] (**SM-6b**), constructed from data of Figure 6;[37,38] $K_{i(16)}$ = 1.75 ± 0.25 μM. Using GSH as a variable substrate, both **8** and **16** showed, predictably, mixed inhibition kinetics, since the lines of the Lineweaver–Burk graph intersected the left of the reciprocal velocity axis (**SM-7a** for **8** and **SM-7b** for **16**).

2.4. Studying the cytotoxic activity of the selected inhibitor lead structures with human colon adenocarcinoma cell line

In the course of lead structure studies, it is useful to evaluate compounds not only on the basis of target enzyme activity, but also on cell-based assays. For the latter application, the human colon adenocarcinoma cell line (Caco2) is a good choice, particularly for this study, because it expresses predominantly the hGSTA1-1 isoenzyme of interest.[13,41,42] Therefore, the four selected compounds, **6**, **8**, **14** and **16**, along with two control structures, benzophenone **5** and ketoxime **11**, were evaluated for their cytotoxicity against Caco2 cells. The results obtained on cell viability (Table 3) indicated that **5** and **11**, the former with respect to **6** and **8** and the latter with respect to **14** and **16**, showed low cytotoxicity (LC$_{50}$ >400 μM for **5**; Figure 7a) and 315 ± 1.4 μM for **11**; Fig. 7d), whereas **6**, **8** and **14** showed significant increase of cytotoxicity (respective LC$_{50}$ values 31.4 ± 0.4 μM (Fig. 7b), 120.0 ± 1.9 μM (Fig. 7c) and 87.0 ± 1.9 μM (Fig. 7e)). Interestingly, of the four inhibitors tested, only **16** displayed very low cytotoxic effect (LC$_{50}$ >400 μM; Fig. 7f), even lower than control structure **11** (LC$_{50}$ 315.0 ± 1.4 μM; Fig. 7d). Therefore, taking into consideration both the cytotoxicity and inhibition profiles (Table 3), one would regard benzophenone **6** and its *N*-carbonyl hydrazone analogue **14**, as an overall better balanced choice for lead structures, since they exhibit satisfactory cytotoxicity (Table 3; LC$_{50(6)}$ = 31.4 ± 0.4 μM; LC$_{50(14)}$ = 87 ± 1.9 μM) and enzyme inhibitory potency (IC$_{50(6)}$ = 1.77 ± 0.10 μM; IC$_{50(14)}$ = 0.33 ± 0.05 μM).

3. Experimental

3.1. Materials and instrumentation

Reagents were used as commercially purchased, while solvents were purified and dried according to standard procedures. Melting points were measured on an Electrothermal IA9000 Series apparatus and are uncorrected. Infrared spectra were recorded on a JASCO FT/IR-5300 spectrometer as KBr discs. Elemental analyses were performed on a Carlo Erba 1106 analyser. NMR spectra were measured on a Bruker Avance 400 MHz and a Varian 600 MHz spectrometers, in CDCl$_3$ or DMSO-d_6 solutions. Mass spectra were recorded by Micromass—Platform LC or JEOL JMS-AX505 W low or high resolution instruments. Analytical TLC was run on Fluka Silica Gel F254. Preparative Flash Chromatography was run on Carlo Erba Reactifis-SDS SILICE 60 A C.C 40–63 μm Chromagel.

3.2. Synthesis of substituted 2,2′-bis-hydroxybenzophenones

Details on the synthesis of the title hydroxybenzophenone derivatives used in the present work have been described earlier by Tsoungas et al.[11,12] The methodology followed is summarized in Scheme 1 whereas the derivatives tested are laid out in Table 1. Briefly, the established[10] reactivity profile of xanthone core structure **1** has been suitably exploited to effect its regioselective substitution. Nucleophilically triggered ring-opening of **4** by alkali, then, generated the corresponding, also regioselectively substituted, target benzophenones **5–10**. If an alkoxide is used, as the cleaving nucleophile, one of the phenolic OH groups in **5** is protected and masked as an alkyl ether. This approach provides a means to differentiate between two otherwise identical aromatic rings and OH groups in **5** and, thus, allow the synthesis of a diverse array of useful derivatives through further transformations. The general method used for ring opening of **4** and spectral data of most active of the tested ketones and previously unreported 2,2′-bis-hydroxybenzophenones **6** and **8** are described herein (FT-IR, ^{1}H NMR and Mass Spectra are given as Supplementary material).

3.2.1. Synthesis of benzophenones 5–10 (general method)

To a solution of xanthone (1 mol equiv) in DMSO, an aqueous solution of 12 N KOH (1.4 mol equiv) is added and the reaction mixture is refluxed in a preheated bath for 12 h. The reaction mixture is then concentrated in vacuo and the residue is treated with ice-water, slowly acidified with concentrated HCl to pH 3 and exhaustively extracted with dichloromethane. The combined extracts are repeatedly washed with water and brine, dried over sodium sulfate, concentrated and the residue is either directly chromatographed (silica, petroleum ether/dichloromethane 6:1) or triturated with an ether/petroleum ether mixture prior to chromatography.

3.2.1.1. 2-Hydroxy-4-phenyl-2′-hydroxybenzophenone (6). Yield: 72%, R_f = 0.64. IR ν_{max}: 3422 (OH), 1615 (C=O), 1594, 1509, 1479 cm^{-1}. ^{1}H NMR (400 MHz, CDCl$_3$): δ (ppm) 7.01–6.92 (3H, m, Ar-H), 7.14–7.11(1H, d, Ar-H J = 8.4 Hz), 7.20–7.17 (1H, d, Ar-H J = 8.4 Hz), 7.38–7.34 (1H, d, Ar-H J = 7.2 Hz), 7.45–7.41 (1H, d, Ar-H, J = 7.6 Hz), 7.57–7.48 (2H, m, Ar-H), 7.70–7.66 (1H, dd, Ar-H, J = 8.0 Hz, J = 1.6 Hz), 7.87–7.74 (1H, dd, Ar-H, J = 8.8 Hz, J = 2.4 Hz), 7.83 (1H, d, Ar-H, J = 2.4 Hz), 10.50 (1H, s, ArOH), 10.64 (1H, s, ArOH). ^{13}C NMR (75.4 MHz, CDCl$_3$): δ (ppm) 199.2, 162.5, 161.5, 141.2, 134.6, 134.2, 134.1, 133.2, 131.8, 129.5, 128.9, 128.2, 127.6, 127.5, 123.5, 120.5, 120.1, 119.5, 118.1. HRMS-ES [M−H$^+$] m/z: found 289.08630, calcd for C$_{19}$H$_{14}$O$_3$ 290.1790.

3.2.1.2. 2-Hydroxy-4-bromo-2′-hydroxybenzophenone (8). Yield: 81%, m.p.128 °C, R_f = 0.59. IR ν_{max}: 3450–3200 (OH), 1621 (C=O), 1609,

1585, 1479 cm^{-1}. ^{1}H NMR (CDCl$_3$): δ (ppm) 7.1–6.9 (2H, m, Ar-*H*), 7.08 (1H, d, Ar-*H*), 7.6–7.5 (3H, m, Ar-*H*), 7.69 (1H, d, Ar-*H J* = 2.4 Hz), 10.49 (1H, s, Ar-*H*), 10.41 (1H, s, Ar-H). ^{13}C NMR (75.4 MHz, CDCl$_3$): δ (ppm) 201.1, 162.3, 161.8, 136.8, 135.7, 133.9, 133.4, 123.8, 121.6, 120.8, 118.9, 117.5, 115.5. HRMS-ES [M$^+$] *m/z*: found 293.030, calcd for C$_{13}$H$_9$BrO$_3$ 293.0220.

3.2.2. Synthesis of oximes 11–13 and hydrazones 14–16

These were prepared by literature methods.[11,12] Spectral data of the most active of the oximes **11** and hydrazones **14** are described herein (FT-IR, ^{1}H NMR and Mass Spectra are given as Supplementary material, **SM**-**8**).

3.2.2.1. 2,2′-Bis-hydroxybenzophenone oxime (11).

Yield: 76%, mp: 113 °C, R_f = 0.58. IR ν_{max}: 3539 (NOH), 3362 (OH), 1620 (C=N) cm^{-1}. ^{1}H NMR (600 MHz, DMSO-d_6): δ (ppm) 7.03–6.71 (4H, m, Ar), 7.28–7.19 (4H, m, Ar), 9.67 (1H, br, OH), 11.60 (2H, br s, NOH and OH). ^{13}C NMR (75.4 MHz, DMSO-d_6): δ (ppm) 158.8, 158.7, 157.4, 130.1, 130.3, 129.7, 129.6, 128.4, 128.2, 128.1, 119.4, 118.6, 116.4. HRMS-ES [M$^+$] *m/z*: found 228.0666 calcd for C$_{13}$H$_{11}$NO$_3$ 228.0666.

3.2.2.2. 2,2′-Bis-hydroxybenzophenone *N*-benzoylhydrazone (14).

Yield: 72%, mp: 236–7 °C, R_f = 0.43. IR ν_{max}: 3317 (NH), 3280 (OH), 1649 (C=O) cm^{-1}. ^{1}H NMR (400 MHz, DMSO-d_6): δ (ppm) 6.81–6.72 (1H, m, Ar*H*), 6.84 (1H, dd, Ar*H*, *J* = 7.6 Hz), 7.05–6.95 (3H, m, Ar*H*), 7.10 (1H, d, Ar*H*, *J* = 8 Hz), 7.2 (1H, dd, Ar*H*, *J* = 7.6 Hz, *J* = 1.6 Hz), 7.35–7.25 (1H, m, Ar*H*), 7.68–7.38 (5H, m, Ar), 10.50 (1H, s, Ar*OH*), 10.18 (1H, s, Ar*OH*), 13.00 (1H, s, NH). ^{13}C NMR (75.4 MHz, DMSO-d_6): δ (ppm) 163.4, 161.2, 161.1, 155.7, 132.9, 132.7, 132.6, 132.5, 130.7, 130.4, 128.9, 128.8, 127.8, 127.6, 121.5, 121.3, 118.5, 118.4, 117.9, 117.8. HRMS-ES [M$^+$] *m/z*: found 332.1089 calcd for C$_{20}$H$_{16}$N$_2$O$_3$ 332.1088.

3.3. Expression and purification of hGSTA1-1

This is based on a published method.[19] Briefly, the expression of GST was induced from *Escherichia coli* BL21 (DE3) cells harbouring the plasmid pET101/D by addition of IPTG. The cells were harvested by centrifugation (845 mg cell paste), resuspended in phosphate buffer, disrupted by sonication and the liquid phase ('supernatant'), containing the enzyme was collected by centrifugation. The GST, from the supernatant, was purified on an affinity chromatography adsorbent bearing the tripeptide glutathione immobilized to cross-linked agarose, previously epoxy-activated with bis-epoxirane (1,4-butanediol diglycidyl ether). Non adsorbed protein was washed off with equilibration buffer, prior to desorbing bound GST in equilibration buffer containing 10 mM glutathione. Fractions with enzyme activity were polled (specific activity $\approx$ 83 enzyme units per mg protein), concentrated (nitrocellulose filter, cutoff 10 kDa) and diluted by dropwise addition of glycerol to 50% (v/v) final concentration (typically 445 enzyme units per mL stock solution). The enzyme solution can be stored at –20 °C for several months without appreciable loss of activity.

3.4. Enzyme assays for testing the compounds as inhibitors for hGSTA1-1

3.4.1. Routine enzyme assay for determining hGSTA1-1 activity

Determination of GST activity was performed by monitoring the formation of the conjugate between CDNB and GSH at 340 nm (ε = 9600 L mole^{-1} cm^{-1}) at 25 °C. An assay volume of 1 mL contained potassium phosphate buffer (100 mM, pH 6.5), 1 µmol of CDNB (33 µL from a 30 mM solution in ethanol) and 2.5 µmol of GSH (33 µL from a 75 mM aqueous solution). DMSO was also added (5 µL, in place of equal volume of buffer) only for control

assays of inhibition experiments with the test compounds (see below). The mixture was incubated at 25 °C for 5 min, prior to adding the enzyme sample. Initial velocities were determined in triplicate and were corrected for spontaneous reaction rates, when necessary. One unit of enzyme activity is defined as the amount of enzyme that produces 1.0 µmol of product per minute under the assay conditions.

3.4.2. Screening the compounds as hGSTA1-1 inhibitors

The screening assay for the test compounds of Table 1 as possible GST inhibitors was implemented by adding the ingredients in the following order (1 mL assay volume): potassium phosphate buffer (100 mM, pH 6.5), 0.75 µmol GSH (prepared in water), 25 nmol test compound (5 µL from a 5 mM solution in DMSO) and enzyme (up to 20 µL of purified GST, typically producing 0.15 ΔA_{340} per min). The mixture was incubated at 25 °C for 1 min, prior to adding 0.3 µmol CDNB (prepared in ethanol). The observed rate was used to calculate the remaining activity (%), taking as 100% initial activity value the rate observed after replacing the test compound by an equal volume of DMSO (5 µL).

3.5. Inhibition studies with purified hGSTA1-1

The GraFit3 version 3 computer program (Erithacus Software, Ltd., U.K.) was used for producing kinetic graphs, determining apparent kinetic parameters/constants and IC$_{50}$ values.

3.5.1. Determination of IC$_{50}$ values for inhibitors 6, 8, 14 & 16

Initial velocities for the GST-catalysed reaction with CDNB and GSH as substrates were measured at 25 °C, in the presence of various concentrations of inhibitors **6**, **8**, **14** & **16**. The assay employed was the same as that for the screening of the test compounds as GST inhibitors (see previous paragraph). Different inhibitor quantities were introduced in the assay mixture in 5 µL DMSO. The observed rate was used to calculate the remaining activity (%), taking as 100% initial activity value the observed rate (approx. 0.15 ΔA_{340}/min) after replacing the inhibitor by an equal volume of DMSO (5 µL). The IC$_{50}$ values were determined from a graph depicting remaining GST activity (%) versus inhibitor concentration.

3.5.2. Kinetic analysis of inhibitors 6, 8, 14 & 16 using CDNB as a variable substrate

Initial velocities for the hGSTA1-1-catalysed reaction with CDNB as variable substrate were determined in reaction mixtures of a total volume of 1 mL (25 °C) containing potassium phosphate buffer (100 mM, pH 6.5), 2.5 mM GSH and different concentrations of CDNB (typically 37.5–980 µM) in the absence and presence of inhibitor **6** (0, 0.50 and 1.70 µM) or inhibitor **8** (0, 0.25 and 0.50 µM) or inhibitor **14** (0, 0.37 and 0.74 µM) or inhibitor **16** (0, 0.05, 0.20 and 0.60 µM).

3.5.3. Kinetic analysis of inhibitors 6, 8, 14 & 16 using GSH as a variable substrate

Initial velocities for the hGSTA1-1-catalysed reaction with GSH as variable substrate were determined in reaction mixtures of a total volume of 1 mL (25 °C) containing potassium phosphate buffer (100 mM, pH 6.5), 1 mM CDNB and different concentrations of GSH (100–2500 µM) in the absence and presence of inhibitor 6 (0, 1.70 and 5.10 µM) or inhibitor 8 (0, 0.5, 0.8 and 1.3 µM) or inhibitor 14 (0, 0.74 and 1.11 µM) or inhibitor 16 (0, 0.4, 0.8 and 1.2 µM).

3.6. Caco-2 cell line culture

Caco-2 cells[42] were grown as monolayer cultures in Dulbecco's Modified Eagle Medium (DMEM) from BIOCHROM supplemented

F. D. Perperopoulou et al. / Bioorg. Med. Chem. 22 (2014) 3957–3970

3969

with 10% v/v fetal bovine serum (GIBCO) 1% v/v penicillin–streptomycin solution (GIBCO) and 1% v/v L-glutamine (GIBCO). The cells were grown in standard conditions until 60–70% confluency and maintained at 37 °C in an incubator with 5% CO_2.

3.7. Cytotoxicity experiments for determining LC_{50} values for Caco-2 cells with compounds 5, 6, 8, 11, 14 & 16

Cytotoxicity was evaluated in Caco-2 cells using the MTT assay, which measures the ability of viable cells to reduce a soluble tetrazolium salt to an insoluble purple formazan precipate.[43] Caco-2 cells used for MTT assay were seeded at a density 1.0×10^4 cells/well in 96-well plates and pre-incubated for 48 h in DMEM containing 10% FBS before the addition of the inhibitors. These were dissolved in 100% DMSO and then diluted with serum-free DMEM as culture medium to different concentrations and added to Caco-2 cells cultured in serum-free medium for an additional 24 h.[44] After removal of the medium, each well was incubated with 0.5 mg/mL MTT (Sigma–Aldrich) in DMEM serum-free medium at 37 °C for 3 h. At the end of the incubation period, the medium was removed and the intracellular formazan was solubilised with 200 μL DMSO and quantified by reading the absorbance at 550 nm on a microplate reader (Optimax, Molecular Devices). Percentage of cell viability was calculated based on the absorbance measured relative to the absorbance of cells exposed to the negative control. The GraphPad PRISM version 5 computer program was used for producing cytotoxicity graphs and determining LC_{50} values.

3.8. Modeling and docking: the in silico structure of hGSTA1-1 and docking of the 2,2′-dihydroxybenzophenones and their N-carbonyl analogues

The structure of hGSTA1-1 in complex with ethacrynic acid and its glutathione conjugate was downloaded from the Protein Data Bank (PDB code 1GSE) and prepared with the Protein Preparation Wizard[45] in Maestro (Schrodinger, LLC, New York, NY). A grid including the tripeptide substrate glutathione was set up centered on ethacrynic acid. The synthetic analogues were docked flexibly using Glide SP.[46,47] Docking results were both visually inspected and quantitatively evaluated based on docking score. In order to study analogue binding in the presence of CDNB, another grid was set up including both the tripeptide substrate glutathione and CDNB, and in silico molecular docking was repeated. Forty different global molecular properties have been predicted for the compounds using QikProp (Schrodinger, LLC, New York, NY). All figures depicting 3D models were created using PyMOL, version 1.4 (Schrodinger, LLC).

4. Conclusions

2,2′-Benzophenones and N-carbonyl analogues have been investigated as inhibitors for the MDR-involved human GST isoenzyme A1–1. 2,2′-Dihydroxybenzophenones **6** and **8** and the N-acylhydrazone analogues **14** and **16** stood out after screening a structure-based library of candidate inhibitors. All four structures showed strong hGSTA1-1 inhibition potency (IC_{50} values in the lower micromolar to sub-micromolar range), interacting at the CDNB-binding site of the enzyme. Furthermore, on account of their cytotoxicity ($LC_{50(6)} = 31.4 \pm 0.4$ μM; $LC_{50(14)} = 87 \pm 1.9$ μM) and enzyme inhibition ($IC_{50(6)} = 1.77 \pm 0.10$ μM; $IC_{50(14)} = 0.33 \pm 0.05$ μM) profiles, benzophenone **6** and its N-acyl hydrazone analogue **14** appear to be promising lead structures.

Acknowledgments

Supplementary data

Supplementary data associated with this article can be found, in the online version, at http://dx.doi.org/10.1016/j.bmc.2014.06.007.

References and notes

1. Acuna, U. M.; Jancovski, N.; Kenelly, E. J. *Curr. Top. Med. Chem.* **2013**, *9*, 1560.
2. Alvarez, C.; Alvarez, R.; Corchete, P.; Pırez-Melero, C.; Pelαez, R.; Medarde, M. *Bioorg. Med. Chem.* **2008**, *16*, 8999. and references cited therein.
3. Terzidis, M. A.; Tsiaras, V. G.; Stephanidou-Stephanatou, J.; Tsoleridis, C. A. *Synthesis* **2011**, 97.
4. Dang, A.-T.; Miller, D. O.; Dawe, L. N.; Bodwell, G. J. *Org. Lett.* **2008**, *10*, 233. and references cited therein.
5. Chen, H.; Xie, F.; Gong, J.; Hu, Y. *J. Org. Chem.* **2011**, *76*, 8495. and references cited therein.
6. Storm, J. P.; Andersson, C.-M. *J. Org. Chem.* **2000**, *65*, 5264. and references cited therein.
7. Kaiser, F.; Schwink, L.; Velder, J.; Schmalz, H.-G. *J. Org. Chem.* **2002**, *67*, 9248.
8. Martin, R. Aromatic Hydroxyketones: Preparation and Physical Properties, 3rd ed., vol. 1, 2011, Springer.
9. Romão, M. J.; Knäblein, J.; Huber, R.; Moura, J. J. G. *Prog. Biophys. Mol. Biol.* **1997**, *68*, 121.
10. Odrowaz-Sypniewski, M. R.; Tsoungas, P. G.; Varvounis, G.; Cordopatis, P. *Tetrahedron Lett.* **2009**, *50*, 5981.
11. Gardikis, Y.; Tsoungas, P. G.; Potamitis, C.; Zervou, M.; Cordopatis, P.; Hornby, J. A.; Hornby, J. A. *Heterocycles* **2011**, *83*, 1077.
12. Gardikis, Y.; Tsoungas, P. G.; Potamitis, C.; Zervou, M.; Pairas, G.; Cordopatis, P. *Heterocycles* **2011**, *83*, 1291.
13. Zoi, O. G.; Thireou, T. N.; Rinotas, V. E.; Tsoungas, P. G.; Eliopoulos, E. E.; Douni, E. K.; Labrou, N. E.; Clonis, Y. D. *J. Biomol. Screen.* **2013**, *18*, 1092.
14. Frova, C. *Biomol. Eng.* **2006**, *23*, 149.
15. Oakley, A. J. *Drug Metab. Rev.* **2011**, *43*, 138.
16. Kodera, Y.; Isobe, K.; Yamauchi, M.; Kondo, K.; Akiyama, S.; Ito, K.; Nakashima, I.; Takagi, H. *Cancer Chemother. Pharmacol.* **1994**, *34*, 203.
17. Sau, A.; Trengo, F. P.; Valentino, F.; Federici, G.; Caccuri, A. M. *Arch. Biochem. Biophys.* **2010**, *500*, 116.
18. Yang, X.; Liu, G.; Li, H.; Zhang, Y.; Song, D.; Li, C.; Wang, R.; Li, B.; Liang, W.; Jing, Y.; Zhao, G. *J. Med. Chem.* **2010**, *53*, 1015.
19. Koutsoumpli, G. E.; Dimaki, V. D.; Thireou, T. N.; Eliopoulos, E. E.; Labrou, N. E.; Varvounis, G. I.; Clonis, Y. D. *J. Med. Chem.* **2012**, *55*, 6802.
20. Axarli, I.; Labrou, N. E.; Petrou, C.; Rassias, N.; Cordopatis, P.; Clonis, Y. D. *Eur. J. Med. Chem.* **2009**, *44*, 2009.
21. Johansson, K.; Ito, M.; Schophuizen, C. M. S.; Thengumtharayil, S. M.; Heuse, V. D.; Zhang, J.; Shimoji, M.; Ang, W. H.; Dyson, P. J.; Shibata, A.; Shuto, S.; Ito, Y.; Abe, H.; Morgenstern, R. *Mol. Pharm.* **2011**, *8*, 1698.
22. Cacciatore, I.; Caccuri, A.; Di Stefano, A.; Luisi, G.; Nalli, M.; Pinnen, F.; Ricci, G.; Sozio, P. *Il Farmaco* **2003**, *58*, 787.
23. Adang, A. E.; Brussee, J.; van der Gen, A.; Mulder, G. J. *J. Biol. Chem.* **1991**, *266*, 830.
24. Razza, A.; Galili, N.; Smith, S.; Godwin, J.; Lancet, J.; Melchert, M.; Jones, M.; Keck, J. G.; Meng, L.; Brown, G. L.; List, A. *Blood* **2009**, *113*, 6533.
25. Abd-El-Aziz, A. S.; Bernardin, S. *Coord. Chem. Rev.* **2000**, *203*, 219.
26. Tlili, A.; Xia, N.; Monnier, F.; Taillefer, M. *Angew. Chem., Int. Ed.* **2009**, *48*, 8725.
27. Yuan, Y.; Thomé, I.; Kim, S. H.; Chen, D.; Beyer, A.; Bonnamour, J.; Zuidema, E.; Chang, S.; Bolm, C. *Adv. Synth. Catal.* **2010**, *352*, 2892.
28. Cox, P. J.; Kechagias, D.; Kelly, O. *Acta Cryst.* **2008**, *B64*, 206.
29. Jaccard, G.; Lauterwein, J. *Helv. Chim. Acta* **1986**, *69*, 1469.
30. Andersen, K. B.; Langgard, M.; Spanget-Larsen, J. *J. Mol. Struct.* **1999**, *509*, 153.
31. Gilli, G.; Gilli, P. The Nature of the hydrogen bond. Outline of a comprehensive H bond theory, Monograph, 2009; Oxford Scholarship online Monographs.
32. Lu, L.; He, L. *J. Mol. Struct.* **2012**, *1010*, 79.
33. Kolev, T.; Stambolyiska, B.; Yancheva, D. *Chem. Phys.* **2005**, *324*, 489.
34. Kolobe, D.; Sayed, Y.; Dirr, H. W. *Biochem. J.* **2004**, *382*, 703.
35. Copeland, R. A. *Anal. Biochem.* **2003**, *320*, 1.
36. Reaction mechanisms incorporating coupled proton and electron transfers (PCET) concertedly, through proton relay, is currently a particularly active field (see Bonin, J.; Constantin, C.; Robert, M.; Savéant, J.-M.; Tard, C. Acc. Chem. Res. **2012**, *45*, 372).
37. Dixon, M.; Webb, E. *Enzymes (3rd ed.)*; Longman Group Ltd: London, UK, 1979; pp 332–381.
38. Leskovac, V. *Comprehensive Enzyme Kinetics*; Kluwer Academic Publishers: New York, USA, 2003; pp 73–94. 95–110, 139–170.
39. Mahajan, S.; Atkins, W. M. *Cell. Mol. Life Sci.* **2005**, *62*, 1221.
40. Sayed, Y.; Hornby, J. A.; Lopez, M.; Dirr, H. *Biochem. J.* **2002**, *363*, 341.
41. Beaumont, P. O.; Moore, M. J.; Ahmad, K.; Payne, M. M.; Lee, C.; Riddick, D. S. *Cancer Res.* **1988**, *58*, 947.
42. Sambuy, Y.; De Angelis, I.; Ranaldi, G.; Scarino, M. L.; Stammati, A.; Zucco, F. *Cell Biol. Toxicol.* **2005**, *21*, 1.

43. Scudiero, D. A.; Shoemaker, R. H.; Paull, K. D.; Monks, A.; Tierne, S.; Nofziger, T. H.; Currens, M. J.; Seniff, D.; Boyd, M. R. *Cancer Res.* **1988**, *48*, 4827.
44. Kowapradit, J.; Opanasopit, P.; Ngawhirunpat, T.; Apirakaramwong, A.; Rojanarata, T.; Ruktanonchai, U.; Sajomsang, W. *AAPS Pharm. Sci. Tech.* **2010**, *11*, 497.
45. Sastry, G. M.; Adzhigirey, M.; Day, T.; Annabhimoju, R.; Sherman, W. J. *Comput. Aid. Mol. Des.* **2013**, *27*, 221.
46. Friesner, R. A.; Banks, J. L.; Murphy, R. B.; Halgren, T. A.; Klicic, J. J.; Mainz, D. T.; Repasky, M. P.; Knoll, E. H.; Shaw, D. E.; Shelley, M.; Perry, J. K.; Francis, P.; Shenkin, P. S. *J. Med. Chem.* **2004**, *47*, 1739.
47. Halgren, T. A.; Murphy, R. B.; Friesner, R. A.; Beard, H. S.; Frye, L. L.; Pollard, W. T.; Banks, J. L. *J. Med. Chem.* **2004**, *47*, 1750.